AGU PUBLICATIONS

JGR

Journal of Geophysical Research: Solid Earth

RESEARCH ARTICLE
10.1002/2016JB013597

Repressurization following eruption from a magma chamber with a viscoelastic aureole

Paul Segall[1]

[1]Department of Geophysics, Stanford University, Stanford, California, USA

Key Points:
- Pressurization of spherical magma chamber with viscoelastic shell following explosive eruption with recharge dependent on chamber pressure
- Posteruption inflation can occur without recharge due to viscoelastic relaxation with relatively incompressible magma
- For short Maxwell times hoop stress changes from compression to tension, favoring dike opening well before chamber pressure recovers

Supporting Information:
- Supporting Information S1

Correspondence to:
P. Segall,
segall@stanford.edu

Citation:
Segall, P. (2016), Repressurization following eruption from a magma chamber with a viscoelastic aureole, *J. Geophys. Res. Solid Earth*, *121*, doi:10.1002/2016JB013597.

Received 27 SEP 2016
Accepted 20 NOV 2016
Accepted article online 24 NOV 2016

Abstract I analyze an approximate solution for spherical magma chambers (radius R_1) surrounded by Maxwell viscoelastic shells (radius R_2) in elastic half-spaces following a sudden decrease in pressure. Mass flux into the chamber is proportional to the pressure difference between a deep source and chamber, $p^\infty - p(t)$. Solutions depend on R_2/R_1, $\mathcal{B} \equiv \beta_c/(\beta_m + \beta_c)$, where β_m, β_c are magma and chamber compressibilities, t_R is the relaxation time, and τ is the recharge time for the elastic system. Without recharge the system exhibits either posteruptive deflation or, for incompressible magmas, partial reinflation. More generally, immediate posteruptive inflation is favored by large $\mathcal{B}$, t_R/τ and small R_2/R_1. With short t_R and large $\mathcal{B}$ the time for magma chamber pressure to recover increases significantly. Posteruptive creep increases the chamber pressure, decreasing the pressure gradient driving recharge, delaying pressure recovery. Following eruption the hoop stresses, which are initially compressive, relax toward the radial stress causing them to go through a local (relative tension) maximum. The magma pressure in excess of the dike normal compression at the chamber wall can recover to preeruptive values well before the chamber pressure or erupted mass recovers. This suggests that dikes could nucleate at the chamber margin well before sufficient pressure has recovered to drive them far from the chamber. For some parameters coeruptive deflation has not fully recovered when the magma overpressure relative to hoop stress in the elastic region is restored to preeruptive values, a condition assumed to be sufficient for eruption.

1. Introduction

Most analyses of volcano deformation assume a pressurized cavity, of some shape, in an elastic half-space [*Mogi*, 1958; *Yang et al.*, 1988; *Fialko et al.*, 2001; *Dzurisin*, 2003; *Segall*, 2013]. Yet the crust surrounding a long-lived magma chamber is subjected to temperatures well above the point where it responds elastically. *Dragoni and Magnanensi* [1989] first analyzed the response of a spherical magma chamber surrounded by a Maxwell viscoelastic shell in an otherwise elastic full space. Their analysis reveals that following a step increase in pressure within the magma chamber, the stresses within the viscoelastic shell relax, transmitting the chamber pressure to the outer boundary of the viscoelastic shell. The displacements in the outer, elastic region thus increase monotonically. The instantaneous, elastic response is that of a pressurized chamber in a fully elastic region with inner radius R_1 (Figure 1), while the fully relaxed (infinite time) response in the outer region is equivalent to a spherical magma chamber with radius of the viscoelastic shell, $R_2 > R_1$. *Segall* [2010, section 7.6] extended the *Dragoni and Magnanensi* [1989] result to an approximate half-space solution, following the approach of *McTigue* [1987] for a pressurized spherical cavity in an elastic half-space. The approximation is expected to be accurate in the limit that the outer radius R_2 is small compared to the depth of the chamber center, d, although *McTigue* [1987] showed that in the elastic case the error is small for modest ratios of chamber radius to depth.

The first-order correction for the free surface increases the displacements on that plane, relative to the full-space solution by a factor of $4(1-\nu)$, where ν is Poisson's ratio [*McTigue*, 1987]. *Newman et al.* [2001], who developed a Finite Element Model (FEM) of a spherical chamber surrounded by a viscoelastic shell in an otherwise elastic half-space, noted that for $\nu = 0.25$, the displacements on the free surface are a factor of 3 greater than the full-space equivalent, exactly as predicted by the first-order correction $4(1-\nu)$. *Newman et al.* [2006] extended the analysis to a prolate ellipsoidal chamber with a surrounding viscoelastic shell and estimated plausible pressure histories to fit geodetic observations at Long Valley caldera.

For a linear viscoelastic medium the surface deformation can be written in terms of a convolution of the magma chamber pressure-rate history with viscoelastic response functions (Appendix A, equation (A22)).

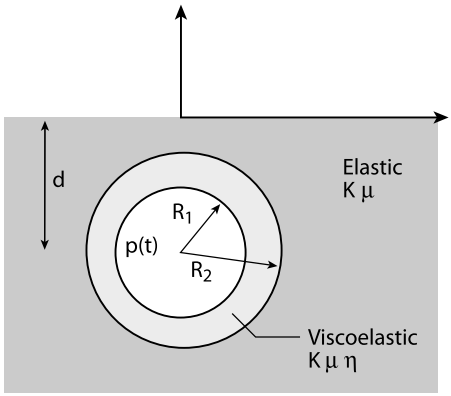

Figure 1. Geometry of a spherical magma chamber with a Maxwell viscoelastic shell. R_1 is the radius of the magma chamber. R_2 is the radius of the viscoelastic shell. Elastic properties are assumed to be the same in both regions, for simplicity.

To deconvolve the viscoelastic response and determine the magma chamber pressure history requires a priori knowledge of the rheological properties of the viscoelastic crust surrounding the chamber. One approach has been to develop thermal models of the crust around the magma chamber and estimate temperature-dependent effective viscosities through rheological models appropriate for the given lithologies. However, the requisite rheological parameters and their dependence on temperature are functions of composition, grain size, activity of water, and strain rate and are thus imperfectly known. *Del Negro et al.* [2009] developed a FEM model of a viscoelastic shell surrounding a spherical magma chamber, in which the viscosity was determined by a steady state thermal model. The viscosity of the crust within the shell depends on temperature, although the thickness of the shell was specified. Fixing rheological parameters, they find viscosities ranging from $\eta = 10^{15}$ Pa s to 10^{20} Pa s for magma chamber temperatures of $T = 1000$°K and from 10^{13} Pa s to 10^{17} Pa s for $T = 1500$°K. For a shear modulus of $\mu = 10^{10}$ Pa this leads to characteristic relaxation times η/μ that range from 10^3 to 10^{10} s, highlighting the difficulty of constraining the viscosity a priori. In comparison, *Newman et al.* [2001] suggest that rhyolites at near solidus temperatures (670°C) have a viscosity of $\eta = 10^{16}$ Pa s, while for quartz-bearing country rock at temperatures of 350°C η ranges between 10^{17} Pa s and 10^{19} Pa s.

Masterlark et al. [2010] employed a model similar to that of *Del Negro et al.* [2009] to study deformation accompanying a months-long eruption of Okmok volcano in Alaska. They developed a steady state thermal model with magma reservoir maintained at 1200°C and assumed a brittle ductile transition at 750°C, such that behavior is assumed to be elastic for $T < 750$°C. This leads to a ratio of outer radius to inner radius, R_2/R_1, of 1.5. They assumed a constant flux of magma out of the chamber during the eruption and solve for the flux and viscosity of the shell that best fits the available geodetic data, yielding an estimated viscosity of 7.5×10^{16} Pa s.

In this paper, I explore analytically the response of the crust to rapid deflation accompanying a short-lived eruption. The advantage of this scenario is that the sudden drop in pressure acts as an impulse that can be used to better resolve the time-dependent response of the medium surrounding the magma chamber, in contrast to inflationary periods where the magma chamber pressure history is unknown. Following the eruption two effects come in to play: (1) viscoelastic relaxation of the rocks surrounding the chamber which, if the chamber were held at fixed pressure, causes continued deflation, and (2) repressurization due to influx of new magma from a deeper source, which causes inflation. It would appear that these effects lead to posteruptive signals of opposite sign. However, I will show that if the magma compressibility is sufficiently low, viscous creep of rock surrounding the chamber causes the pressure to increase, even if there is no recharge into the chamber. Perhaps, counter intuitively, this can lead to posteruptive inflation even in the absence of influx of new magma.

It has also been suggested that viscoelastic relaxation acts to surpress diking from the magma chamber as melt accumulates, allowing much larger magma reservoirs to develop [*Jellinek and DePaolo*, 2003; *Karlstrom et al.*, 2010]. Analysis of the growth of super volcano sized magma chambers is not accessible with the small strain model considered here, which does not include stoping, wall-rock melting, or finite deformations.

It is further assumed here that magma chamber recharge, as well as viscous relaxation, occurs on timescales much shorter than the timescales over which the thermal field evolves. Nevertheless, it is informative to consider the effect of viscous relaxation on the stress field surrounding the magma chamber and the implications for dikes exiting the chamber. I find that for short relaxation times compared to the characteristic time for magma recharge the hoop stresses within the viscoelastic shell actually favor dike opening well before the magma chamber pressure recovers.

2. Method

The model is illustrated schematically in Figure 2. The magma chamber is fed by a deep source that is assumed to be sustained at constant pressure. The magma pressure at the centroid of the chamber is p. Label p^∞ the chamber pressure in magmastatic equilibrium with the source region, i.e., $p_{\text{deep}} = p^\infty + \rho g H$, where ρ is the magma density and H is the vertical distance between the source region and the chamber centroid. Prior to the eruption, the magma chamber may be inflating such that $p(t = 0^-) \equiv p_0^- \leq p^\infty$.

I assume that stresses in the initial, preeruptive, state (Figure 2a) are in quasi-static equilibrium with gravitational body forces and the pressure of magma within the chamber, p_0^-. Deviatoric stresses within the viscoelastic shell surrounding the magma chamber may be partially or fully relaxed depending on the Maxwell relaxation time relative to the time since the previous eruption. Stress perturbations and displacements are measured relative to this initial, equilibrated state. This procedure neglects higher-order contributions to the equilibrium equations due to changes in density, perturbations in the gravitational potential, and the advected prestress, which are expected to be small [e.g., *Dahlen and Tromp*, 1998; *Segall*, 2010, Chapter 9].

During an eruption mass is evacuated from the chamber (assumed instantaneously) such that the pressure drops to $p_0^- + \delta p(t = 0^+)$, where $\delta p(t = 0^+) < 0$ is proportional to the erupted mass (see below). The shell surrounding the magma chamber initially responds elastically, but with time two things happen: magma flows from the deep source into the chamber, and the viscoelastic shell relaxes. Treating the magma chamber as a lumped parameter, conservation of mass, m, (assuming small changes) requires

$$\frac{dm}{dt} = \frac{d(\rho V)}{dt} = \rho V \beta_m \frac{dp}{dt} + \rho \frac{dV}{dt} = q_{\text{in}} - q_{\text{out}}, \tag{1}$$

where ρ is the magma density in the initial state, V is the initial magma chamber volume, $\beta_m = (1/\rho)\partial\rho/\partial p$ is the magma compressibility, and q are mass flow rates. Following the eruption, there is no outflow, such that $q_{\text{out}} = 0$. I assume the flux into the chamber is proportional to the pressure difference, $q_{\text{in}} = \Omega(p^\infty - p)$, where Ω is a conductivity parameter with units kg Pa^{-1}s^{-1} [e.g., *Mastin et al.*, 2008]. Combining

$$\Omega(p^\infty - p) = \rho \left(V \beta_m \frac{dp}{dt} + \frac{dV}{dt} \right). \tag{2}$$

The magma chamber pressure p can be written as

$$p(t) = p_0^- + \delta p(t) \tag{3}$$

where p_0^- is the chamber pressure at $t = 0^-$ immediately prior to the eruption, and $\delta p(t)$ is the change in pressure, both during and following the eruption. Substituting (3) into (2) yields

$$\Omega \left[p^\infty - p_0^- - \delta p(t) \right] = \Omega[\Delta p_0 - \delta p(t)] = \rho \left(V \beta_m \frac{dp}{dt} + \frac{dV}{dt} \right), \tag{4}$$

where $\Delta p_0 \equiv p^\infty - p_0^-$.

For elastic deformation of the surrounding crust the volume change of the chamber is proportional to the pressure change, $dV/dt = V\beta_c dp/dt$, where β_c is an effective chamber compressibility. For the special case of a spherical cavity far from the Earth's surface

$$\beta_c = \frac{3}{4\mu} \tag{5}$$

[e.g., *Segall*, 2010, equation (7.13)], such that (4) reduces to

$$\Delta p_0 - \delta p(t) = \tau \frac{d\delta p}{dt} \quad \text{with} \quad \tau \equiv \frac{\rho V(\beta_m + \beta_c)}{\Omega}. \tag{6}$$

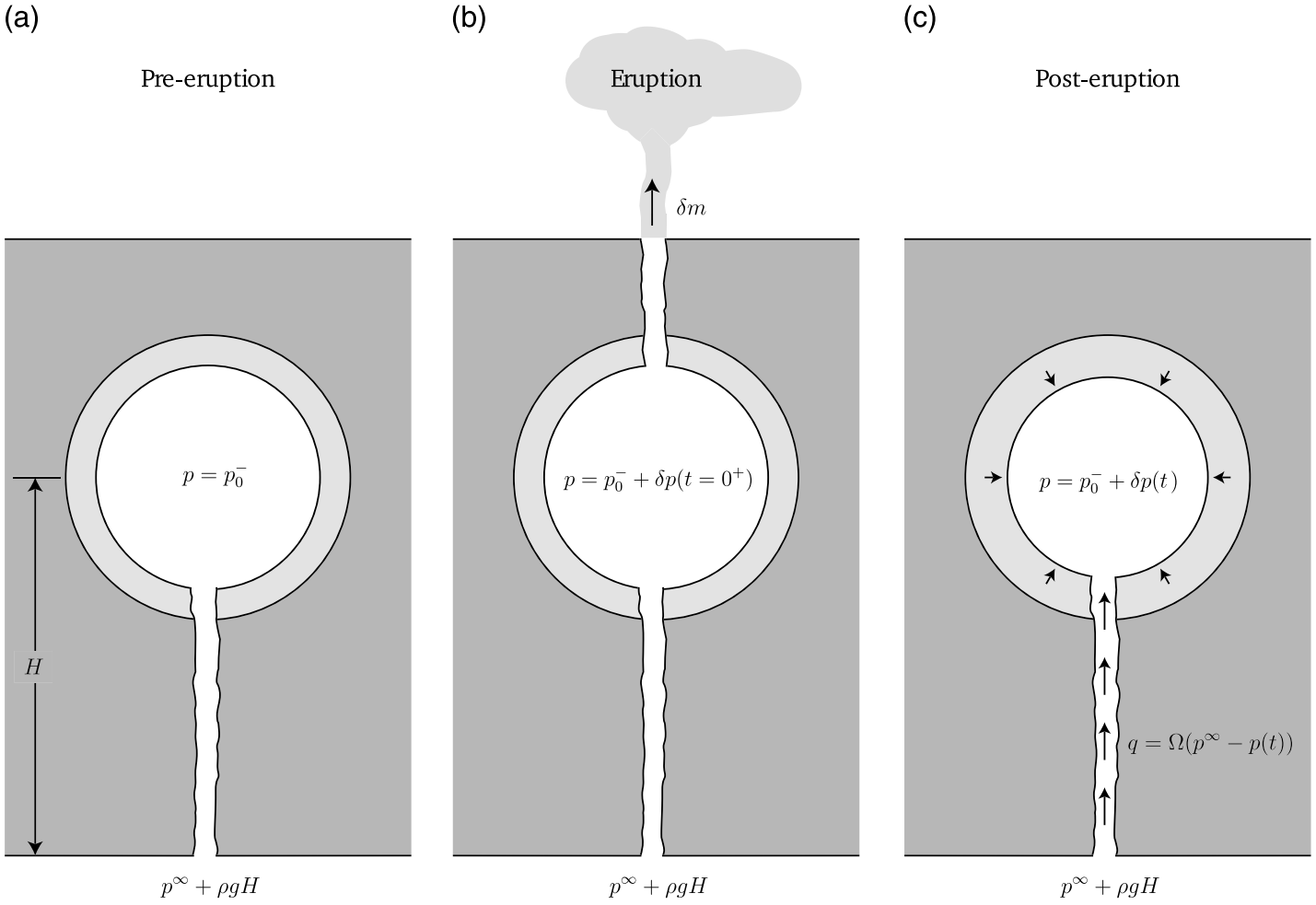

Figure 2. Schematic of magma system. (a) Preeruptive state, with magma chamber pressure p_0^- and deep reservoir at pressure $p_{\text{deep}} = p^\infty + \rho g H$. (b) Coeruptive state, mass δm is erupted causing the chamber pressure to drop to $p_0^- + \delta p(t = 0^+)$. Viscoelastic shell surrounding magma chamber responds elastically. (c) Posteruptive state, magma flows into the chamber from deep reservoir, viscoelastic shell deforms, both contributing to a time-dependent pressure $p_0^- + \delta p(t)$.

For $\Delta p_0 - \delta p > 0$ magma flows into the chamber causing the pressure to increase, with a characteristic refilling time, τ. Flow into the magma chamber ceases when $\delta p = \Delta p_0 = p^\infty - p_0^-$.

In the viscoelastic case the volume of the magma chamber changes due both to creep closure and refilling. Neglecting free-surface effects on the displacements of the chamber wall, the rate of chamber volume change is approximately

$$\frac{dV}{dt} \simeq 4\pi R_1^2 \frac{d}{dt} u_r(r = R_1), \tag{7}$$

where u_r is the radial displacement, and R_1 is the magma chamber radius (Figure 1). Substituting (7) into (4) yields

$$\Omega[\Delta p_0 - \delta p(t)] = \rho \left[V \beta_m \frac{dp}{dt} + 4\pi R_1^2 \frac{d}{dt} u_r(r = R_1) \right]. \tag{8}$$

The solution to (8) is given in Appendix A using Laplace transform methods. This yields the change in magma chamber pressure as a function of time

$$\delta p(t) = \frac{\Delta p_0 t_R^{-1}}{\tau s_1 s_2} + \frac{\left(\Delta p_0 + s_1 \tau \delta p_0^+\right)\left(s_1 + t_R^{-1}\right)}{s_1 \tau (s_1 - s_2)} e^{s_1 t} + \frac{\left(\Delta p_0 + s_2 \tau \delta p_0^+\right)\left(s_2 + t_R^{-1}\right)}{s_2 \tau (s_2 - s_1)} e^{s_2 t}, \tag{9}$$

where the roots s_1, s_2 are given by

$$s_{1,2} = -\frac{t_R^{-1}(1+\mathcal{B}\alpha)+\tau^{-1}}{2} \pm \frac{1}{2}\sqrt{\left(t_R^{-1}(1+\mathcal{B}\alpha)+\tau^{-1}\right)^2 - 4\tau^{-1}t_R^{-1}} \tag{10}$$

and

$$t_R = \frac{3\eta(1-\nu)}{\mu(1+\nu)}\left(\frac{R_2}{R_1}\right)^3 \tag{11}$$

$$\alpha = \frac{3(1-\nu)}{(1+\nu)}\left[\left(\frac{R_2}{R_1}\right)^3 - 1\right] \tag{12}$$

$$\mathcal{B} = \frac{\beta_c}{\beta_m + \beta_c}. \tag{13}$$

Here t_R is the relaxation time for the system [*Dragoni and Magnanensi*, 1989], and $\mathcal{B}$ is a dimensionless ratio of magma and chamber compressibilities. Assuming Poisson's ratio is known, the fundamental unknown parameters are $\mathcal{B}, \eta/\mu, R_2/R_1$, and τ, or alternatively, $\mathcal{B}, R_2/R_1, t_R$, and τ.

In Appendix A, the limits of (9) are verified to be $\delta p(t = 0^+) = \delta p_0^+$ and $\delta p(t \to \infty) = \Delta p_0$, the latter corresponding to $p(t \to \infty) = p^\infty$ such that recharge ceases. I also show there that in the limit of infinite relaxation time, $t_R^{-1} \to 0$, and equation (9) reduces to the elastic case of a chamber repressurizing due to magma influx. In this limit

$$\delta p_e(t) = \Delta p_0 + \left(\delta p_0^+ - \Delta p_0\right) e^{-t/\tau}, \tag{14}$$

which is immediately seen to be the solution to (6). The other limit, of no magma recharge, $\tau^{-1} \to 0$, is discussed below. First, consider the displacements at the free surface. Following the derivation in Appendix A, the vertical displacements on the free surface can be approximated by

$$u_z(z=0,t) = \frac{(1-\nu)R_1^3}{\mu d^2}\left\{\frac{\Delta p_0 (R_2/R_1)^3}{\tau s_1 s_2 t_R} + \frac{\left(\Delta p_0 + s_1\tau\delta p_0^+\right)\left[s_1 + t_R^{-1}(R_2/R_1)^3\right]}{s_1\tau(s_1-s_2)}e^{s_1 t} + \frac{\left(\Delta p_0 + s_2\tau\delta p_0^+\right)\left[s_2 + t_R^{-1}(R_2/R_1)^3\right]}{s_2\tau(s_2-s_1)}e^{s_2 t}\right\}\left[\frac{1}{(1+\zeta^2)^{3/2}}\right]. \tag{15}$$

Here $\zeta = h/d$ is the radial distance from the center of the source, h, normalized by the source depth, d. (Note that I have omitted the superscript $^{(2)}$, denoting the elastic region 2, for notational simplicity.) As discussed in Appendix A, the approximation should be accurate as long as the depth of the magma chamber centroid is reasonably large compared to the radius of the viscoelastic shell, R_2. This parallels the well-known Mogi solution for a spherical magma chamber in a fully elastic half-space that is accurate as long as the centroid depth is small compared to the chamber radius R_1. The radial horizontal displacements are found by replacing the factor $1/(1+\zeta^2)^{3/2}$ with $\zeta/(1+\zeta^2)^{3/2}$ [e.g., *Segall*, 2010, chapter 7]. Appendix A verifies that the instantaneous displacements at $t = 0$ are proportional to $\delta p_0^+ R_1^3$, while at $t \to \infty$ the displacements are proportional to $\Delta p_0 R_2^3$.

Equation (15) shows that the surface deformation is the sum of exponentials with two time constants, corresponding to $-1/s_1$ and $-1/s_2$. These time constants arise from the interaction of viscous relaxation, with characteristic time t_R and magma recharge, with characteristic time τ, although from equation (10), $-1/s_1$ and $-1/s_2$ generally do not correspond individually to these times. (The exception, as discussed in Appendix A, is for $\mathcal{B} = 0$ where the roots $s_{1,2}$ correspond to $-\tau^{-1}$ and $-t_R^{-1}$.) Interestingly, several studies have shown that deformation following some eruptions requires two distinct time constants [*Nooner and Chadwick*, 2009; *Reverso et al.*, 2014]. Additional analysis will be required to determine whether these observations are sensibly described by the simple model presented here.

3. Surface Deformation

If the eruption is of sufficiently short duration the response will be completely elastic. In this case the pressure change due to eruption of mass δm is, from (1) and the definition of β_c,

$$\delta p_0^+ = \frac{\delta m}{\rho V(\beta_m + \beta_c)}. \tag{16}$$

δm is negative, such that there is an instantaneous pressure drop; however, pressure may partly recover with time as the surroundings relax and the chamber squeezes inward.

3.1. No Recharge Limit

An interesting limiting case is when there is no influx into the magma chamber. In the limit $\tau^{-1} \rightarrow 0$, equation (A15) in Appendix A can be inverted analytically, yielding

$$\delta p(t)_{\lim \tau^{-1}\rightarrow 0} = \frac{\delta p_0^+}{1+\mathcal{B}\alpha}\left\{1 + \mathcal{B}\alpha \exp\left[-(1+\mathcal{B}\alpha)t/t_R\right]\right\}. \tag{17}$$

Note that the characteristic time for the no recharge limit is $t_R/(1+\mathcal{B}\alpha)$ and thus depends on relative compressibility and size of the viscoelastic shell as well as intrinsic Maxwell time η/μ.

Inversion of (A18) in Appendix A yields the displacements

$$u_z(z=0,t)_{\lim \tau^{-1}\rightarrow 0} = \frac{(1-\nu)R_1^3}{\mu d^2}\frac{\delta p_0^+}{1+\mathcal{B}\alpha}\left\{\left(\frac{R_2}{R_1}\right)^3 - \left[\left(\frac{R_2}{R_1}\right)^3 - 1 - \mathcal{B}\alpha\right]\exp\left[-(1+\mathcal{B}\alpha)t/t_R\right]\right\} \times \left[\frac{1}{(1+\zeta^2)^{3/2}}\right]. \tag{18}$$

The instantaneous displacement due to the eruption is

$$u_z(z=0,t=0)_{\lim \tau^{-1}\rightarrow 0} = \frac{(1-\nu)\delta p_0^+ R_1^3}{\mu d^2}\left[\frac{1}{(1+\zeta^2)^{3/2}}\right], \tag{19}$$

which is of course the *Mogi* [1958] solution for a change in pressure δp_0^+. The fully relaxed, infinite time, response is

$$u_z(z=0,t\rightarrow\infty)_{\lim \tau^{-1}\rightarrow 0} = \frac{(1-\nu)\delta p_0^+ R_1^3}{\mu d^2}\frac{(R_2/R_1)^3}{1+\mathcal{B}\alpha}\left[\frac{1}{(1+\zeta^2)^{3/2}}\right]. \tag{20}$$

The fully relaxed response (20) also has the same form as the Mogi solution; however, the amplitude of the displacement is modified. From equations (19) and (20) the ratio of displacement at infinite to zero time is

$$\frac{u(t\rightarrow\infty)}{u(t=0)} = \frac{(R_2/R_1)^3}{1+\mathcal{B}\alpha} = \frac{(R_2/R_1)^3}{1+\frac{3(1-\nu)}{(1+\nu)}\mathcal{B}\left[\left(\frac{R_2}{R_1}\right)^3 - 1\right]}, \tag{21}$$

which is illustrated in Figure 3. Values greater than one indicate continued posteruptive subsidence, while values less than one indicate posteruptive inflation. Highly compressible magma favors continued posteruption subsidence, while the reverse is true for relatively incompressible magmas. The amplitude of the posteruptive changes increases with increasing R_2/R_1 in both cases.

Whether the final subsidence exceeds the coeruptive subsidence depends on whether the ratio in (21) is greater or less than 1. From (21) posteruptive deflation occurs when $\mathcal{B} < (1+\nu)/3(1-\nu)$; for $\nu = 1/4$ this ratio is $5/9 \approx 0.56$, as seen in Figure 3. For larger values of $\mathcal{B}$ (relatively incompressible magmas) the final displacement is less than the immediate posteruptive deflation, that is the coeruptive deflation partially recovers. Notice also that for $\nu = 0.5$, and $\mathcal{B} = 1$, $u(t\rightarrow\infty) = u(t=0)$; in this case both the magma and the surrounding are incompressible, and there is no change in volume as the viscoelastic shell relaxes.

These results can be understood by considering the effect of magma compressibility. For highly compressible magma ($\mathcal{B} \rightarrow 0$) chamber pressure remains constant, and we approach the limit in *Dragoni and Magnanensi* [1989]. As the viscous shell relaxes the pressure boundary condition is transmitted to the outer boundary R_2,

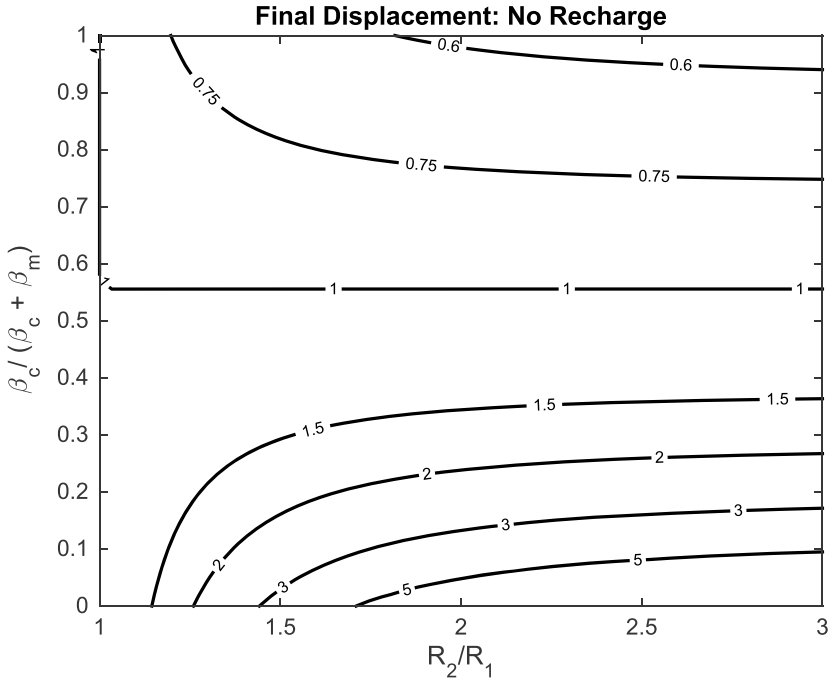

Figure 3. Amplitude of the final displacement relative to the instantaneous posteruptive displacement as a function of relative compressibility and the relative radius of the viscoelastic shell, in the absence of recharge. Values less than 1.0 indicate partial reinflation, whereas values greater than 1.0 indicate continued deflation. $\nu = 0.25$.

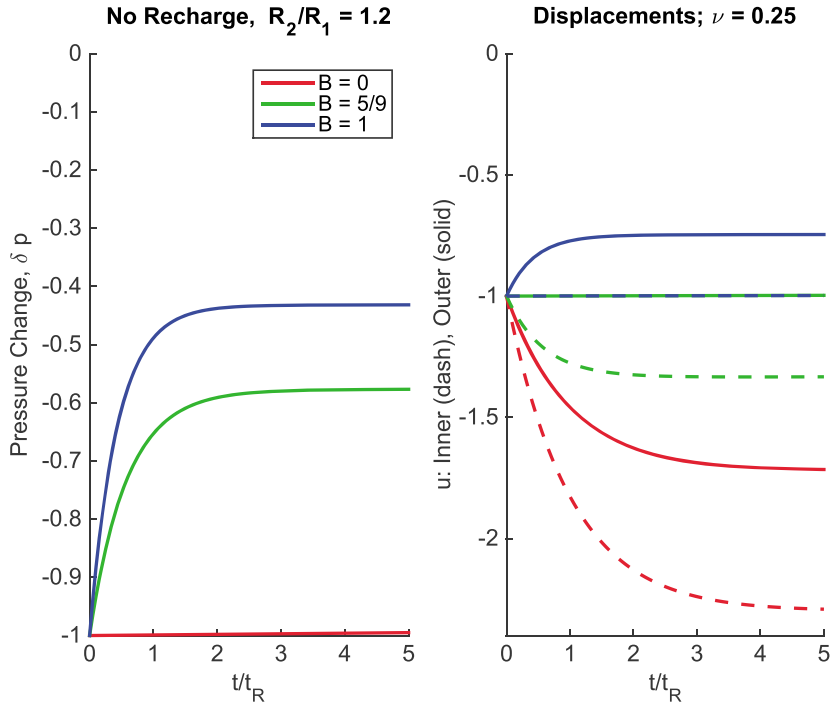

Figure 4. No recharge limit. (left) Normalized chamber pressure. (right) Normalized displacement on inner (dashed) and outer (solid) radii of the viscoelastic shell. For infinitely compressible magma, the chamber pressure is constant following eruption and the coeruption subsidence continues. For an incompressible magma, the chamber pressure partially recovers and there is partial reinflation following the eruption. $\nu = 0.25$, $R_2/R_1 = 1.2$.

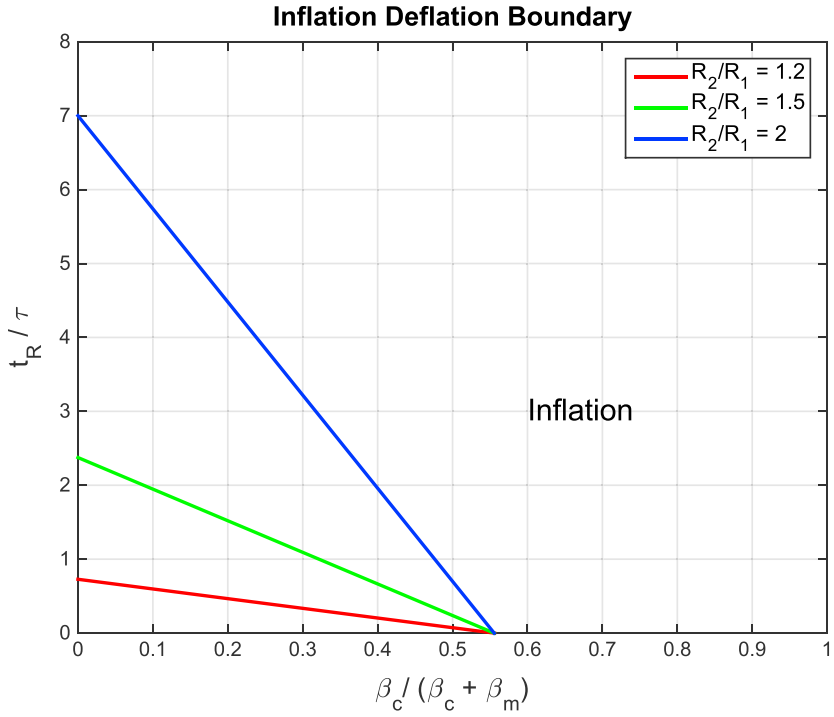

Figure 5. Boundary between instantaneous posteruptive inflation and deflation for different values of R_2/R_1. Values to the right and above the line experience immediate posteruptive inflation. The limit of $t_R/\tau = 0$ corresponds to the no recharge limit.

which has the effect of increasing the amplitude of the coeruptive deflation. For less compressible magmas the pressure increases as the shell creeps inward; in the limit $\mathcal{B} \to 1$, the magma volume is fixed and the shell can only relax outward. In general, the posteruptive displacements are a combination of these two effects: (a) the change in chamber pressure and (b) the relaxation of the surrounding viscoelastic shell. In the $\mathcal{B} \to 0$ limit the latter effect dominates and there is continued deflation following the eruption. In the $\mathcal{B} \to 1$ limit the pressure recovery dominates and there is partial posteruptive rebound.

This limiting behavior is illustrated in Figure 4. For the infinitely compressible magma, $\mathcal{B} = 0$, the pressure is constant, and the system experiences posteruptive deflation. As the shear stresses in the shell relax the radial stress becomes uniform; the resulting extensional strain causes the inner boundary to displace more than the outer boundary. For incompressible magma, $\mathcal{B} = 1$, the pressure partially recovers and the system experiences posteruptive inflation, even without recharge into the magma chamber. In this case, the inner boundary is fixed and relaxation causes the outer boundary to displace outward. For the special case of $\mathcal{B} = (1+\nu)/3(1-\nu) = 5/9$, for $\nu = 0.25$, the inner boundary displaces inward compressing the magma, but the outer boundary experiences no posteruptive displacement.

3.2. Posteruptive Inflation Versus Deflation

The previous discussion considers whether or not the posteruptive response is inflation or deflation for the special case of no recharge into the magma chamber. In this section I consider this question for the more general case including melt influx from the deep reservoir.

The boundary between immediate posteruption deflation and inflation is found from the time derivative of the displacements at $t = 0^+$. Setting $\dot{u}_r^{(2)}(r, t = 0) = 0$ divides parameter space between posteruption inflation and deflation. Here the superscript $^{(2)}$ indicates the outer, elastic region (see Appendix A). This leads to

$$\Delta p_0 - \delta p_0^+ + \delta p_0^+ \frac{\tau}{t_R}\left[\left(\frac{R_2}{R_1}\right)^3 - 1\right]\left[1 - \frac{3(1-\nu)}{(1+\nu)}\mathcal{B}\right] = 0. \tag{22}$$

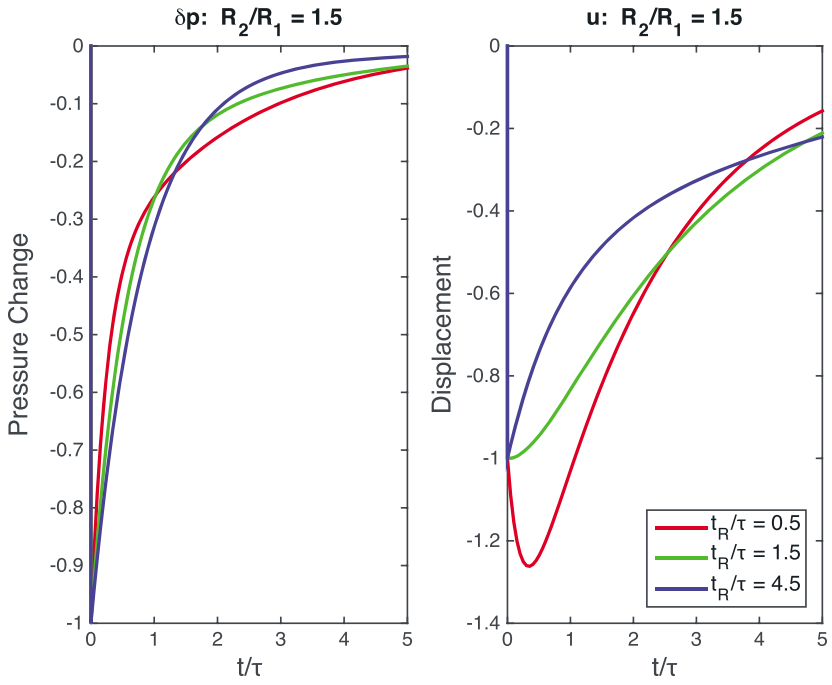

Figure 6. (left) Pressure and (right) displacement for $R_2/R_1 = 1.5$ and $\mathcal{B} = 0.2$. y axis scales are normalized by the coeruptive pressure and displacement changes, respectively.

Assuming relatively low rate of preeruptive inflation such that $\Delta p_0/\delta p_0^+ \ll 1$, equation (22) reduces to

$$\frac{t_R}{\tau} = \left[\left(\frac{R_2}{R_1}\right)^3 - 1\right]\left[1 - \frac{3(1-\nu)}{(1+\nu)}\mathcal{B}\right]. \tag{23}$$

The boundary between posteruptive inflation and deflation depends on τ/t_R as well as R_2/R_1, ν, and $\mathcal{B}$. Note that the ratio t_R/τ can be considered as a Deborah number, the ratio of relaxation time to observation time. The result is shown graphically in Figure 5, for three ratios of R_2/R_1. The no recharge limit corresponds to the $t_R/\tau = 0$ axis. As expected posteruptive reinflation is favored by large $\mathcal{B}$ and t_R/τ, that is short refilling time relative to the Maxwell time. For smaller R_2/R_1 the deflationary field is more restricted.

Sample time histories are shown in Figure 6. From Figure 5, I estimate that for $R_2/R_1 = 1.5$ and $\mathcal{B} = 0.2$ the critical ratio is $t_R/\tau \approx 1.5$. Longer relaxation times lead to inflation, whereas shorter relaxation times lead to deflation. Indeed, as seen in Figure 6, for $t_R/\tau < 1.5$ the initial response is deflationary whereas for $t_R/\tau > 1.5$ the response is immediate inflation.

These results have clear implications for the interpretation of posteruption deformation signals. If inflation is observed immediately following an eruption that would imply a lower bound on t_R/τ, the bound depending on R_2/R_1 and $\mathcal{B}$. Assuming that a priori information can be used to constrain these parameters, one should be able to constrain t_R/τ. For example, thermal models place constraints on R_2/R_1 [*Newman et al.*, 2001; *Masterlark et al.*, 2010], and comparison of eruptive flux to GPS station velocity allows constraints to be placed on the magma system compressibility [*Segall*, 2013; *Hreinsdóttir et al.*, 2014].

4. Eruption Recovery Time

By assumption, the conditions for eruption were met at $t = 0^-$. It is therefore sensible to assume that the subsequent eruption occurs when some combination of magma pressure and stress state in the surrounding crust return to the conditions at $t = 0^-$. If eruption onset requires pushing a plug out of a preexisting conduit, then magma chamber pressure is the dominant factor. For dike propagation, a combination of pressure and stress is relevant to eruption onset (see section 4.2).

If the magma chamber was inflating prior to the eruption (potentially very slowly), then $\Delta p_0 = p^\infty - p_0^- > 0$. In this case the magma chamber pressure recovers to the preeruptive value in a finite time t_c. For an elastic

system this is given by setting δp in equation (14) to zero

$$t_{ce} = \tau \ln\left(1 - \frac{\delta p_0^+}{\Delta p_0}\right), \tag{24}$$

where $\delta p_0^+ < 0$, as the pressure drops during the eruption. For $-\delta p_0^+/\Delta p_0 \gg 1$, $t_{ce} \approx \tau \ln(|\delta p_0^+|/\Delta p_0)$. Because of exponentially decreasing flux in the limit $\Delta p_0 \to 0$ the recovery time in this limit is infinite. For the general viscoelastic case the time for pressure to recover is found by setting δp in equation (9) to zero and solving for t_c.

4.1. Mass Recharge Time

An interesting question is how much magma accumulates in the time interval it takes for the pressure to recover. From (1) and (4)

$$\begin{aligned}\frac{dm}{dt} &= \frac{\rho V(\beta_m + \beta_c)}{\tau}[\Delta p_0 - \delta p(t)] \\ &= \frac{\delta m}{\tau}\left[\frac{\Delta p_0 - \delta p(t)}{\delta p_0^+}\right],\end{aligned} \tag{25}$$

where I have made use of (6) and (16), and δm is the mass loss in the previous eruption. The posteruptive mass change is found by integrating (25)

$$m(t) = \frac{\delta m}{\tau}\left[\frac{\Delta p_0}{\delta p_0^+}t - \int_0^t \frac{\delta p(t')}{\delta p_0^+}\mathrm{d}t'\right]. \tag{26}$$

In the elastic (long Maxwell time) limit the pressure history is given by equation (14). Substituting into (26) yields

$$\frac{m(t)}{\delta m} = \left(1 - \frac{\Delta p_0}{\delta p_0^+}\right)\left(e^{-t/\tau} - 1\right). \tag{27}$$

Setting $m(t) = -\delta m$ yields t_{ce} as in equation (24) as expected; for elastic deformation the mass and pressure changes are proportional.

One can develop approximations for the pressure and mass recovery times accurate in the limit $t_R/\tau \ll 1$, for which the roots, the inverse characteristic relaxation times, are given by $s_1 = -(1+\mathcal{B}\alpha)/t_R$ and $-1/(1+\mathcal{B}\alpha)\tau$. In this limit the characteristic time for both pressure and magma chamber mass to recover is

$$t_c \approx (1+\mathcal{B}\alpha)\tau \ln\left[1 - \frac{\delta p_0^+}{(1+\mathcal{B}\alpha)\Delta p_0}\right], \tag{28}$$

which exceeds the repressurization time in the elastic limit, t_{ce}.

Results are shown for $\Delta p_0/|\delta p_0^+| = 0.05$ in Figure 7. The time for pressure and mass to recover in the elastic case is, $t_{ce} \approx 3.04\tau$. For $t_R/\tau = 0.1$ rapid viscoelastic relaxation substantially delays the pressure recovery, in the case of $\mathcal{B} = 0.8$ by more than a factor of 2 (Figure 7b). In this sense viscoelastic deformation may delay the eruption onset as suggested by *Jellinek and DePaolo* [2003]. In the opposite limit, for $t_R/\tau = 10$ the pressure history is well approximated by (24), while the mass takes considerably longer to recover (Figure 7c). In particular, at the time the pressure has recovered to its preeruption state, only slightly more than 80% of the mass erupted has recovered (Figure 7c).

Figure 8a illustrates the time for magma pressure to recover normalized by t_{ce} as a function of t_R/τ and $\mathcal{B}$, while Figure 8b shows the fraction of the erupted mass that has been recharged at the time pressure recovers to its preeruption value. Figure 8a shows that for $t_R/\tau \ll 1$ and incompressible magmas viscoelastic relaxation increase the time it takes for pressure to recover to its preeruptive value, consistent with equation (28). Interestingly, for $t_R/\tau \sim 10$ and large $\mathcal{B}$, the pressure recovers slightly faster than in the elastic limit. This part of parameter space is associated with incomplete mass recharge at the time the magma pressure has recovered to preeruptive values, as seen in Figures 8b and 7c.

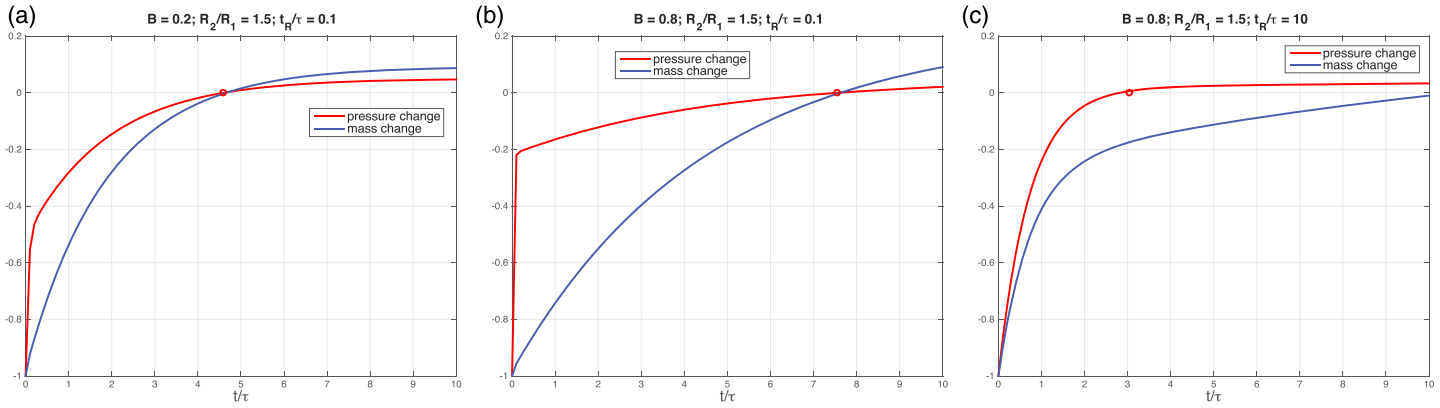

Figure 7. Normalized magma chamber pressure and mass recovery. (a) $t_R/\tau = 0.1$ and $\mathcal{B} = 0.2$. Circle marks the approximation given by equation (28). (b) Same but for $\mathcal{B} = 0.8$. (c) $t_R/\tau = 10$ and $\mathcal{B} = 0.8$. Circle marks the elastic recovery time, t_{ce} given by (24).

This behavior can be understood as follows: for $t_R/\tau \ll 1$ the chamber creeps inward increasing the pressure, which then diminishes the pressure gradient driving flow into the magma chamber. This occurs on the timescale $t_R/(1+\mathcal{B}\alpha)$. The resulting inflation is slow enough that the viscoelastic shell stays relaxed and inflation takes place on a timescale $(1+\mathcal{B}\alpha)\tau$. These two timescales can be seen in Figures 7a and 7b. At the other extreme $t_R/\tau \gg 1$ deformation is essentially elastic, and pressure and mass reaccumulate on timescale t_{ce}. At intermediate t_R/τ viscoelastic relaxation and recharge take place on comparable timescales. For relatively incompressible melts viscoelastic relaxation drives up the chamber pressure, causing the pressure to recover more rapidly than in the elastic case, and also before recharge has replaced the mass lost in the previous eruption.

Traditionally, surface deformation ("inflation") has been monitored to track the state of the magmatic system. In the elastic limit inflation is, of course, proportional to the change in magma chamber pressure. This is compared for the viscoelastic case in Figure 9a, which shows the displacement amplitude within the elastic domain, region 2, at the time magma chamber pressure recovers to preeruptive values, $\delta p(t) = 0$. Interestingly, for t_R/τ between 1 and 10 inflation does not recover to the preeruptive state at the time that pressure recovers, particularly for small $\mathcal{B}$, although this behavior is also observed for relatively incompressible magmas.

Figure 10 shows magma pressure and mass, as well as displacements on the outer boundaries of the magma chamber and the viscoelastic shell as a function of time. For $t_R/\tau \sim 3$ and $\mathcal{B} = 0$, the magma chamber walls continue to creep inward following the eruption (Figure 10a). However, in this perfectly compressible limit

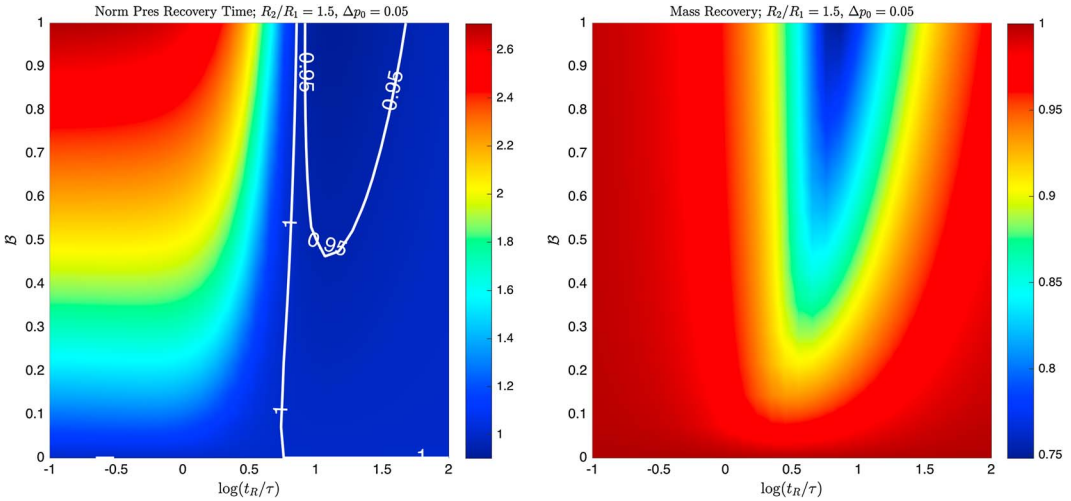

Figure 8. (a) The time it takes for magma chamber pressure to recover to the value prior to the eruption, normalized by the elastic response, $\tau \ln\left(1 - \delta p_0^+/\Delta p_0\right)$. (b) The magma chamber mass that has recovered at the time the pressure recovers to preeruption value; 1.0 equals full mass recovery.

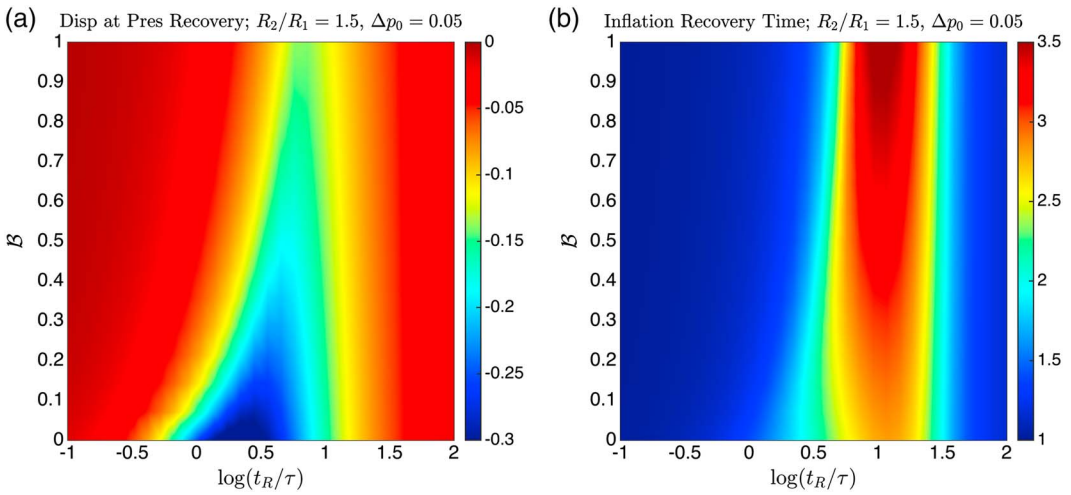

Figure 9. (a) Displacement at the time the pressure recovers to preeruption value; zero corresponds to displacements recovering to preeruption values. (b) Time it takes for remote displacements to recover to preeruptive value normalized by the pressure recovery time.

creep does not alter the chamber pressure, so the magma chamber pressure and mass recovery are proportional (Figures 10a and 8b along the $\mathcal{B} = 0$ axis). Nevertheless, the inward creep of the chamber walls retards reinflation within the elastic domain, region 2. In the incompressible limit, $\mathcal{B} = 1$, the change in mass is proportional to the displacement of the magma chamber walls (Figure 10b). Because the viscoelastic displacements are convolutions over past pressure-rate history, they remain sensitive to the coeruptive pressure drop and thus do not recover as rapidly as the pressure, which increases due both to compression and recharge.

Figure 9b illustrates the time it takes for inflation to recover to its preeruptive value relative to the time for the magma chamber pressure to recover. For large and small t_R/τ this ratio is near one, but for $t_R/\tau \sim 10$ the deformation can take several multiples of the pressure recovery time to restore the coeruptive deflation. This can also be seen in Figure 10, where the displacements in the outer region, $u^{(2)}$, take considerably longer to recover to zero than the chamber pressure. For volcanoes in which magma chamber pressure alone controls eruption potential, systems with parameters similar to those in Figure 10 could be capable of erupting well

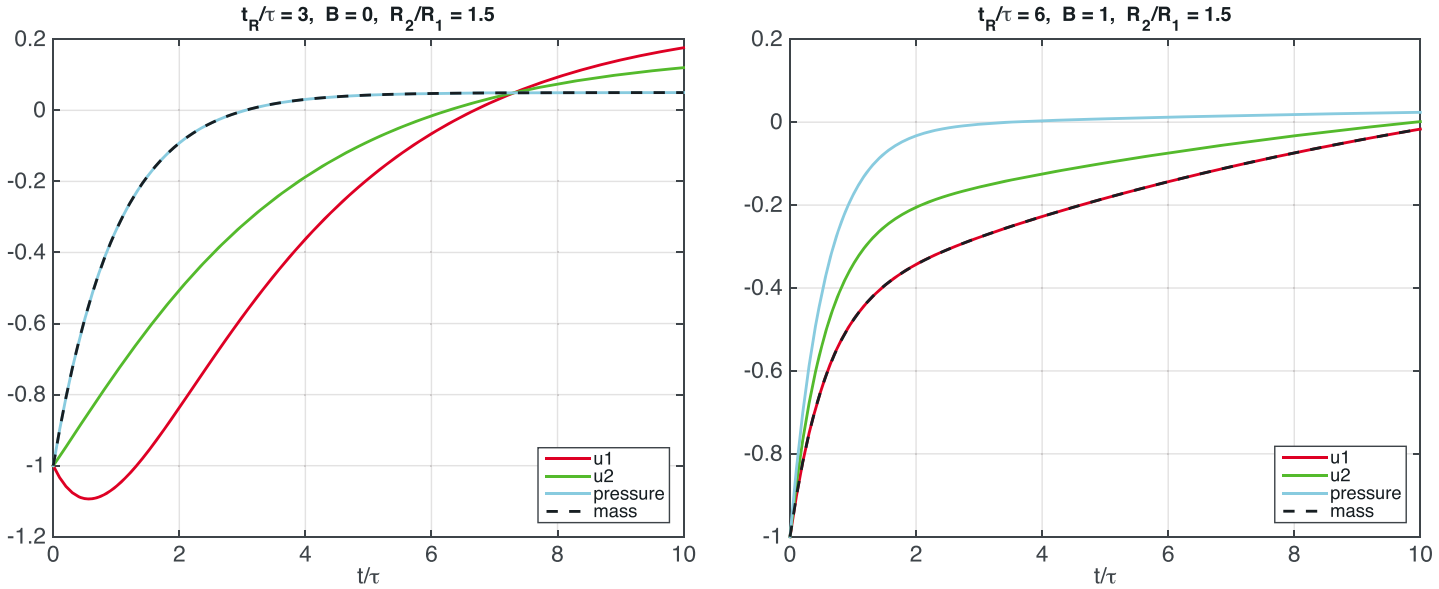

Figure 10. Time dependent behavior when t_R and τ are similar. $u1$ displacement of magma chamber wall, $u2$ displacement of elastic region. (a) $t_R/\tau = 3, \mathcal{B} = 0$. (b) $t_R/\tau = 6, \mathcal{B} = 1$.

before the deflation from the previous eruption had recovered. For eruptions initiated by dike propagation we need to consider stress changes in the crust surrounding the magma chamber, as in the following section.

4.2. Stresses

The magma chamber pressure is determined by a combination of refilling and pressurization due to creep. These factors both contribute to the stresses in the viscoelastic shell and surrounding elastic medium. Appendix A derives the stresses in a full space, that is, ignoring free-surface effects. Based on discussion there, the results are accurate to order $(R_2/d)^2$ and thus should be accurate for modest R_2/d. Indeed, *McTigue* [1987, Figure 2b] shows that in the elastic case ($R_2 = R_1$) the stresses are dominated by the spherically symmetric, full-space solution, even for $R_1/d = 0.5$.

Before exploring general results, which are given in Appendix A, it is worthwhile considering limiting behavior. The short and long time limits are found by substituting (A10) into (A23) and (A24) and applying the limit theorems for Laplace transforms. This yields the instantaneous elastic response: the radial stress is $\sigma_{rr}^{(1)}(t=0) = \sigma_{rr}^{(2)}(t=0) = -\delta p_0^+ (R_1/r)^3$, while the hoop stress is $\sigma_{\theta\theta}^{(1)}(t=0) = \sigma_{\theta\theta}^{(2)}(t=0) = \delta p_0^+/2(R_1/r)^3$, which is half the magnitude but opposite in sign. An expanding (or contracting) sphere in an elastic full space generates pure deviatoric stress. Note by symmetry that $\sigma_{\phi\phi} = \sigma_{\theta\theta}$. The fully relaxed response within the viscoelastic shell is $\sigma_{rr}^{(1)} = \sigma_{\theta\theta}^{(1)} = -\Delta p_0$, the principal stresses become equal, while the radial stress necessarily matches the pressure boundary condition.

It is also useful to consider the no recharge limit. Equation (A26) in Appendix A invert to

$$\sigma_{\theta\theta\ \lim \tau^{-1}\to 0}^{(1)} = \frac{\delta p_0^+}{(1+\mathcal{B}\alpha)}\left\{\left[\frac{(1+\mathcal{B}\alpha)}{2}\left(\frac{R_1}{r}\right)^3 + 1\right] e^{-(1+\mathcal{B}\alpha)t/t_R} - 1\right\}$$
$$\sigma_{rr\ \lim \tau^{-1}\to 0}^{(1)} = \frac{\delta p_0^+}{(1+\mathcal{B}\alpha)}\left\{\left[1 - (1+\mathcal{B}\alpha)\left(\frac{R_1}{r}\right)^3\right] e^{-(1+\mathcal{B}\alpha)t/t_R} - 1\right\}. \tag{29}$$

The stress at $t = 0$ is as noted above, while the fully relaxed response is $\sigma_{\theta\theta}^{(1)}(t\to\infty) = \sigma_{rr}^{(1)}(t\to\infty) = -\delta p_0^+/(1+\mathcal{B}\alpha)$. A significant result is that the hoop stresses within the viscoelastic shell change sign with time. For a drop in chamber pressure during the eruption $\delta p_0^+ < 0$, the hoop stresses are at first compressive, while the radial stress is relative tension. As the shear stresses within shell relax the principal stresses must approach one another. The radial stress is constrained by the pressure boundary condition at $r = R_1$. Thus, the hoop stress changes sign to match the radial stress, in the no recharge limit becoming $-\delta p_0^+/(1+\mathcal{B}\alpha)$, which for $\delta p_0^+ < 0$ is relative tension.

In the limit of long Maxwell relaxation time ($t_R/\tau \gg 1$) we expect the chamber to pressurize exponentially and the circumferential compression to relax exponentially over time. On the other hand, in the limit of slow refilling ($t_R/\tau \ll 1$) the chamber pressure first follows the no recharge limit. For slow refilling we thus expect the hoop stress to change sign. Figure 11 confirms this, showing that the radial stress decays monotonically, while the hoop stress initially decays toward the radial stress, such that the two principal stresses are equal at a time that scales with t_R. The hoop stress then goes through a relative tensile maximum, which may have significant implications for dikes emanating from the chamber. At later time the hoop stress exceeds the radial stress, following which both stresses decay to background values.

The conditions for a dike propagating from the magma chamber to reach the surface depend on magma pressure and viscosity, as well as the surrounding stress and thermal state. The flow rate through the dike must be high enough that the dike can propagate before freezing, and this depends on magma chamber pressure among other parameters. *Rubin* [1993] examines the question of whether a two-dimensional dike can widen elastically fast enough to prevent the walls from freezing inward. For melt initially at the solidus and a linear decay in temperature away from the chamber boundary, the condition for thermal viability depends on a single dimensionless parameter that depends on temperature gradient, the square root of melt viscosity, and the chamber pressure (assumed constant) to the 5/2 power. Thus, the chamber pressure is critical in controlling whether a nascent dike can escape the magma chamber.

In order for a dike propagating away from the magma chamber to even open the pressure within the dike must exceed the least compressive stress tangential to the chamber wall. Here stress and $\delta p(t)$ are measured relative to an initial state which, by assumption, was at eruption. Thus, regardless of the absolute chamber pressure and tectonic stress, $\sigma_{\theta\theta}^{(1)}(r = R_1, t) + \delta p(t)$, measures the difference between the circumferential compressive

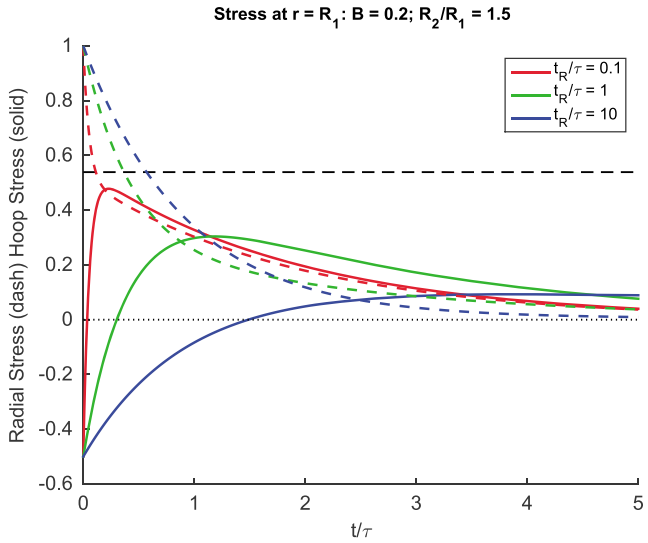

Figure 11. Normalized radial (dashed) and hoop (solid) stress evaluated at the margin of the magma chamber ($r = R_1$) for three different values of t_R/τ. Horizontal dashed line marks the fully relaxed response in the limit of no recharge.

stress and dike pressure, *relative to the past eruptive state*. If conditions at $t = 0^-$ were sufficient to open a dike, those conditions are replicated when $\sigma^{(1)}_{\theta\theta}(r = R_1, t) + \delta p(t) = 0$. Note that dike opening could have occurred before this, as the excess pressure is likely to be positive before recovering to the value it was prior to the previous eruption.

The change in excess pressure is shown in Figure 12, for $\Delta p_0 = 0.05$. Interestingly, the overpressure exceeds the initial, preeruptive value at times on the order of the relaxation time, t_R. Note from Figures 7 and 12 that the excess pressure recovers more rapidly than the pressure, due to the rapid changes in the hoop stress. In the limit $t_R/\tau \ll 1$ the time of the peak excess pressure is

$$t_{\text{cep}} \approx -t_R/(1 + \mathcal{B}\alpha) \ln\left[\frac{(t_R/\tau)^2}{(1 + \mathcal{B}\alpha)^4}\right]. \tag{30}$$

For the parameters in Figure 7a (i.e., $\mathcal{B} = 0.2$), this yields $t_{\text{cep}} \sim 0.38\tau$ compared to the time for magma chamber pressure to recover, given by (28), $t_c \sim 4.6\tau$. This may indicate that the conditions for a dike to open

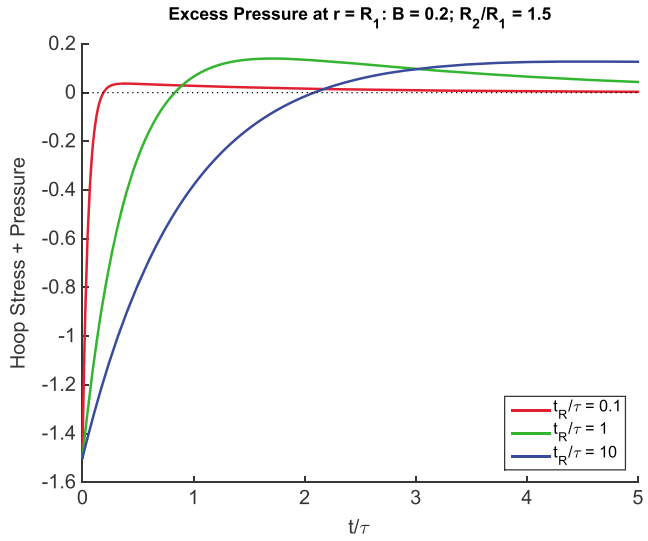

Figure 12. Excess pressure at the margin of the magma chamber $\sigma^{(1)}_{\theta\theta}(r = R_1, t) + \delta p(t)$ for three different t_R/τ. $\Delta p_0 = 0.05$.

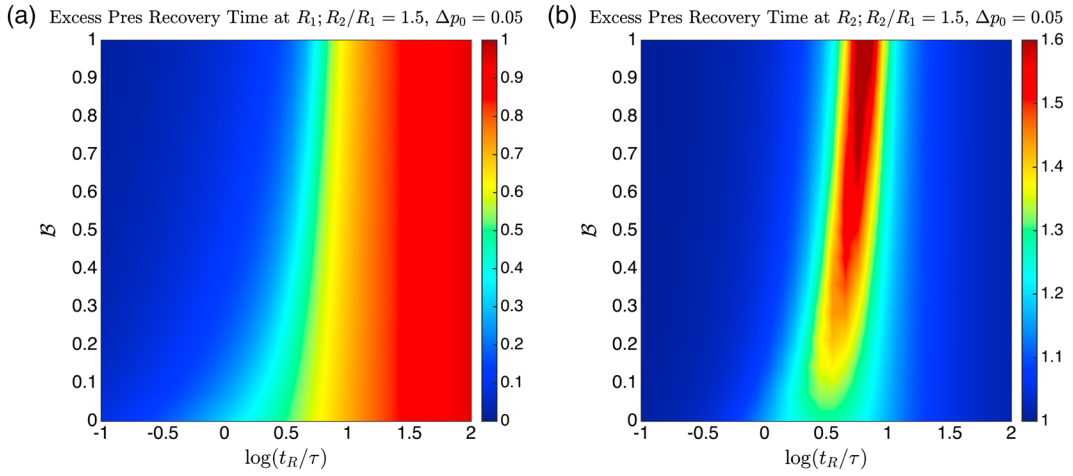

Figure 13. The time it takes for the excess pressure $\sigma^{(1)}_{\theta\theta}(r,t) + \delta p(t)$ to recover to preeruption value, normalized by the time it takes the magma chamber pressure to recover. (a) Excess pressure measured at the edge of the magma chamber $r = R_1$. (b) Excess pressure measured at the edge of viscoelastic shell $r = R_2$.

may occur well before the magma chamber pressure has recovered sufficiently for the dike to be thermally viable according to the criterion outlined by *Rubin* [1993].

Figure 13a illustrates the time it takes for the excess pressure at $r = R_1$ to recover relative to the time for the magma chamber pressure to recover. Again, this serves to emphasize that for $t_R \ll \tau$ the conditions for dike opening may occur well before the magma pressure recovers to a value sufficient for sustained dike propagation. The excess pressure at the chamber wall could permit dike opening, while hoop stresses farther away in the elastic region are still compressive. Figure 13b shows the excess pressure recovery time at the margin of the viscoelastic region $r = R_2$, $\sigma^{(2)}_{\theta\theta}(r = R_2, t) + \delta p(t)$; for intermediate values of t_R/τ the excess pressure in the surrounding elastic region takes *longer* to recover than the chamber pressure.

Finally, Figure 14 shows the excess pressure as a function of radial distance, r, at three critical times: The first is the time at which the excess pressure at $r = R_1$ recovers to the preeruptive state, t_{cep}. Interestingly, the hoop stress is uniform within the viscoelastic zone, region 1, at this time. This can be shown to be a general property that holds for all choices of parameters. At this time the excess pressure in the outer elastic region is

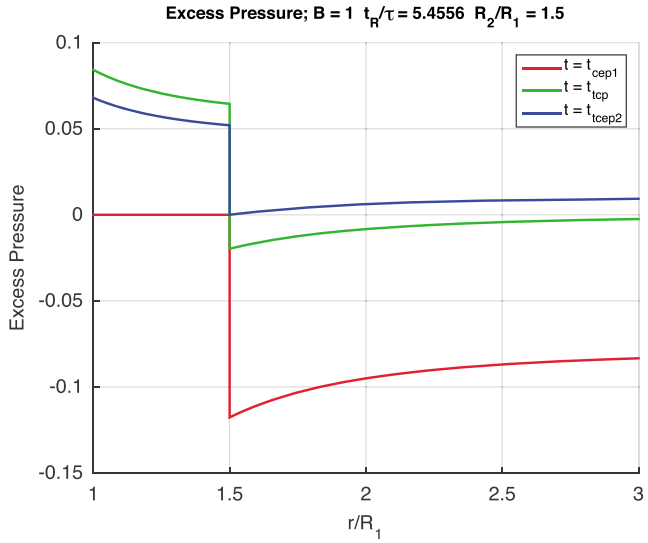

Figure 14. Excess pressure at three critical times: (1) when excess pressure recovers in the inner, viscoelastic shell, t_{cep1}, (2) when the magma pressure recovers, t_{cp}, and (3) when the excess pressure recovers at the outer edge of the viscoelastic shell, t_{cep2}. $\mathcal{B} = 1.0$; $t_R/\tau = 5.455$; $R_2/R_1 = 1.5$.

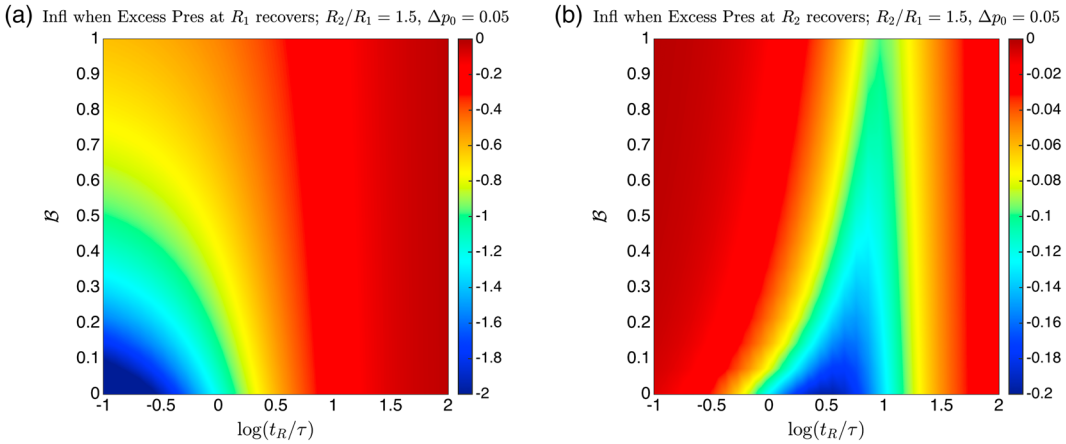

Figure 15. The amount of deflation remaining when excess pressure recovers in (a) region 1 and (b) region 2. Zero equals full recovery.

still compressive, so that presumably a dike might stall after leaving the viscoelastic shell. The second time is when the magma chamber pressure recovers to preeruptive value, t_{cp}. At this time the excess pressure change within the viscoelastic region is everywhere positive, that is exceeding the value prior to the last eruption; however, it is still negative within the outer elastic region. The final time is when the excess pressure recovers at the outer boundary of the viscoelastic region, t_{cep2}. At this time the excess pressure has met or exceeded the value it obtained prior to the last eruption for all distances r.

As discussed above, deformation at Earth's surface is commonly employed as a proxy for the state of the magmatic system. It is thus useful to consider the fraction of the deflation that has recovered when the excess pressure is restored in both the viscoelastic and elastic regions. Figure 15a shows the remaining deflation at the time the excess pressure at the boundary of the magma chamber recovers, t_{cep}. Note that values less than 1.0 in the lower left indicate that the system deflated following the eruption, even though the excess pressure recovered. Figure 15b shows the remaining deflation at the time the excess pressure recovers at the outer margin of the viscoelastic region, t_{cep2}. It resembles Figure 9a which shows the deflation when the magma pressure recovers, although the magnitudes are smaller in Figure 15b. This is because the hoop stresses in the elastic region are compressive, so it takes longer for the excess pressure to recover.

Note from Figure 14 that at $t = t_{cep2}$ the excess pressure is everywhere at least equal to that at the time of the previous eruption. Yet Figure 15b shows that for these parameters, $\log(t_R/\tau) = 0.7368$, $\mathcal{B} = 1$, the deflation from the previous eruption will not have fully recovered at that time. Thus, the conditions for dike propagation may precede recovery of the previous deflation, assuming the magma pressure is sufficiently high to sustain dike growth.

5. Discussion

The approach here has been to find exact solutions to a highly simplified problem. Consequently, a number of rather stringent idealizations have been made: that the magma chamber is spherical, the rheology is Maxwell viscoelastic and spatially uniform within a spherical shell surrounding the magma chamber, and that the radius of that shell is fixed. The latter may not be too restrictive of an approximation, given that the temperature field likely evolves slowly compared to the eruption cycle time. More realistic modeling would account for nonlinear and temperature (and therefore spatially) dependent rheology. I have also assumed the flux is linearly proportional to the difference between a constant source pressure and the magma chamber pressure. This assumption is consistent with Newtonian flow through conduits of fixed dimension and is preferable to assuming a time invariant flux. On the other hand, this may not be a good description if the magma chamber is recharged by dikes intersecting the magma chamber from below [*Karlstrom et al.*, 2009].

The calculations include only a first-order approximation of free-surface effects on the displacement and stress fields. In particular, I approximate the stresses near the magma chamber by the full-space solution and neglect higher-order effects due to the presence of the free surface (section 1). While this should be a reasonable first approximation [e.g., *McTigue*, 1987], *Karlstrom et al.* [2010], who model a similar 2-D plane-strain system using

bipolar coordinates, find a change in the spatial pattern of stress within the viscoelastic shell as deviatoric stresses relax. A more accurate accounting of free-surface effects is an important goal of future work.

In this work I have restricted attention to eruptions with duration that is very short compared to either the relaxation or elastic refilling time, such that the eruption is effectively instantaneous. This should be a good approximation for explosive eruptions that last hours to perhaps a few days. For longer duration effusive eruptions it would be necessary to account for both relaxation and recharge during the course of the eruption. If one were to specify the mass discharge history from (e.g., satellite) observations, the pressure and deformation response could be developed in the form of convolutions over time of the solutions given here for instantaneous mass discharge.

Many of the specific calculations here take the ratio of the shell radius to chamber radius, R_2/R_1, to be 1.5, based on the steady state thermal model of *Masterlark et al.* [2010]. For less mature magmatic systems, for which the temperature field is far from steady state, it is likely the effective viscoelastic shell radius is considerably smaller. Results are qualitatively similar for smaller R_2/R_1, although the magnitude of the viscoelastic effects are diminished. It is also possible that the viscoelastic aureole is composed, at least in part, of partially or recently solidified magma. In this case the shell is likely to be thicker at the bottom than the sides or top. The response of more complex magma reservoir geometries with nonspherical viscoelastic aureoles could be addressed numerically.

I have identified cases where the conditions for dike propagation appear to be met before the deflation accompanying the past event has fully recovered (Figure 15). This has been observed, for example, at Krafla [e.g., *Sturkell et al.*, 2006]. The opposite is also observed, inflation exceeding the deflation of the previous eruption, for example, at Hekla [*Sturkell et al.*, 2013, Figure 7]. The latter is not predicted by any of the models considered here, although I have neglected the influence of changes in tectonic stress that might occur between eruptions. For example, an increase in the least compressive stress would inhibit diking.

Figure 12 shows that for $t_R < \tau$ the excess pressure can recover quickly, due to rapid changes in the hoop stress. At the time the excess pressure at the chamber margin recovers to the preeruptive state the hoop stress is uniform within the viscoelastic shell (Figure 14). This suggests that incipient dikes might be able to propagate into the viscoelastic shell rather early in the reinflationary period. This would transfer heat into the crust surrounding the magma chamber, acting to keep the effective viscosity of the wall rocks low.

It would be interesting to consider at what point the evolving stress field in the elastic region might trigger seismicity. Of course, the tendency for fault slip depends on the total stress state, not simply the perturbing stresses due to magma chamber reinflation. Thus, we cannot predict the onset time for seismicity without additional information. The second stress invariant of the perturbing stresses in the elastic region J_2 depends only on the difference between the radial and hoop stresses. Since $\sigma_{\theta\theta}$ and σ_{rr} are proportional, $\sqrt{J_2}$ is proportional to σ_{rr}, specifically $\sqrt{J_2} = \sqrt{3}\sigma_{rr}/2$. The time dependence of stress in the elastic region is proportional to displacement there, so depending on the threshold for the onset of seismicity, measurable inflation may precede seismicity, consistent with some observations.

6. Conclusions

1. Posteruption inflation can occur without recharge into the magma chamber if the magma is sufficiently incompressible relative to the surroundings.
2. More generally, whether the immediate posteruptive response is deflationary or inflationary depends on magma compressibility $\mathcal{B}$, the ratio of Maxwell time to characteristic chamber refilling time t_R/τ, and the relative size of the viscoelastic aureole, R_2/R_1. Posteruptive inflation is favored by incompressible magmas, long relaxation times, and small viscoelastic aureoles.
3. Fast viscoelastic relaxation delays recovery of the magma chamber pressure and mass relative to the elastic case, particularly for relatively incompressible magmas.
4. For relaxation times roughly an order of magnitude longer than the elastic refilling time, the erupted mass is not fully replaced at the time the magma chamber pressure recovers to the preeruptive state.
5. For relaxation times 1 to 10 times the elastic refilling time, the coeruptive deflation is not fully recovered at the time the magma chamber pressure recovers to the preeruptive state.
6. For relatively short Maxwell relaxation times the radial stress decays monotonically, while the hoop stresses change from relative compression to relative tension. This causes the excess pressure at the chamber wall,

the sum of chamber pressure and hoop stress, to recover to preeruptive values well before the magma chamber pressure recovers.

7. At the time the excess pressure recovers at the chamber wall it is uniform everywhere within the viscoelastic shell (neglecting free-surface effects). This suggests that incipient dikes may open well before the magma pressure is high enough for them to propagate outside the viscoelastic aureole. Such dike injections would transfer heat into the surrounding crust, keeping the effective viscosity of the wall rocks low.
8. For some parameters the hoop stress plus chamber pressure can exceed that at the time of the previous eruption at all distances from the magma chamber before the deflation from the previous eruption has fully recovered. This suggests that the conditions for dike propagation may precede recovery of the coeruptive deflation.

Appendix A: Derivation

Taking Laplace transforms of (8) yields

$$\Omega\left(\frac{\Delta p_0}{s}-\widehat{\delta p}\right)=\rho\left[V\beta_m\left(s\widehat{\delta p}-\delta p_0^+\right)+4\pi R_1^2\left(s\hat{u}-u_0^+\right)\right]. \tag{A1}$$

Here $\hat{\cdot}$ indicates Laplace transform quantity with s the transform variable, and $\hat{u}$ is shorthand for the transform of the radial displacement evaluated on the chamber wall, $\hat{u}\equiv\mathcal{L}[u_r(r=R_1)]$. Also, δp_0^+ is the pressure drop at $t=0^+$ due to the eruption, and u_0^+ is the accompanying radial displacement of the chamber wall. *Dragoni and Magnanensi* [1989] derive the solution for a spherical magma chamber surrounded by a Maxwell viscoelastic shell in a full space. The displacements within the shell, region 1, and the outer, elastic domain, region 2, in the Laplace domain are

$$\begin{aligned}\hat{u}_r^{(1)}(r,s)&=\frac{\hat{A}(s)r}{3}+\frac{\hat{B}(s)}{r^2}\\ \hat{u}_r^{(2)}(r,s)&=\frac{\hat{C}(s)}{r^2}\end{aligned} \tag{A2}$$

where

$$\begin{aligned}\hat{A}&=-\frac{\widehat{\delta p}}{2\eta}\left(\frac{1-2\nu}{1-\nu}\right)\left(\frac{R_1}{R_2}\right)^3\hat{D}^{-1}\\ \hat{B}&=\frac{\widehat{\delta p}R_1^3}{4\mu}(s+\mu/\eta)\hat{D}^{-1}\\ \hat{C}&=\frac{\widehat{\delta p}R_1^3}{4\mu}\left[s+\frac{\mu(1+\nu)}{3\eta(1-\nu)}\right]\hat{D}^{-1}\end{aligned} \tag{A3}$$

and

$$\hat{D}=s+\frac{\mu(1+\nu)R_1^3}{3\eta(1-\nu)R_2^3}\equiv s+t_R^{-1}, \tag{A4}$$

and the relaxation time is

$$t_R=\frac{3\eta(1-\nu)}{\mu(1+\nu)}\left(\frac{R_2}{R_1}\right)^3. \tag{A5}$$

See also Chapter 7 of *Segall* [2010] for derivation. For simplicity, I have restricted results to the case in which the elastic constants are the same in both regions 1 and 2. Because elastic moduli are temperature dependent there could well be a difference, however, this effect is unlikely to be large.

From the *Dragoni and Magnanensi* [1989] results above we find $\hat{u}_r^{(1)}(r=R_1,s)\equiv\mathcal{L}[u_r(r=R_1)]$,

$$\hat{u}\equiv\mathcal{L}[u_r(r=R_1)]=\frac{\widehat{\delta p}R_1}{4\mu}\left(\frac{s+(\alpha+1)t_R^{-1}}{s+t_R^{-1}}\right), \tag{A6}$$

where I have introduced the parameter α

$$\alpha=\frac{3(1-\nu)}{(1+\nu)}\left[\left(\frac{R_2}{R_1}\right)^3-1\right]. \tag{A7}$$

The initial, elastic displacement accompanying the eruption is given by $u_0^+ = \delta p_0^+ R_1/4\mu$. Substituting this and (A6) into (A1) yields

$$\frac{\Omega}{\rho}\left(\frac{\Delta p_0}{s} - \widehat{\delta p}\right) = V\beta_m\left(s\widehat{\delta p} - \delta p_0^+\right) + V\beta_c\left[s\widehat{\delta p}\left(\frac{s+(\alpha+1)t_R^{-1}}{s+t_R^{-1}}\right) - \delta p_0^+\right], \tag{A8}$$

where I have made use of the definition of the chamber compressibility (5). Note that the elastic limit of (A8), found by setting $t_R^{-1} \to 0$, yields the Laplace transform of the elastic governing equation (6). Separating the elastic response yields

$$\frac{\Delta p_0}{s} - \widehat{\delta p} = \tau\left[s\widehat{\delta p} - \delta p_0^+ + \mathcal{B}s\widehat{\delta p}\left(\frac{\alpha t_R^{-1}}{s+t_R^{-1}}\right)\right], \tag{A9}$$

where I have introduced the dimensionless parameter $\mathcal{B}$, defined in (13), and the characteristic refilling time τ, defined in (6). Solving for $\widehat{\delta p}$ yields

$$\widehat{\delta p}(s) = \frac{\left(\Delta p_0 + s\tau\delta p_0^+\right)\left(s+t_R^{-1}\right)}{s\left[\tau s\mathcal{B}\alpha t_R^{-1} + (\tau s+1)\left(s+t_R^{-1}\right)\right]}. \tag{A10}$$

The limit theorems for Laplace transforms are used to verify that $\delta p(t=0^+) = \delta p_0^+$ and $\delta p(t\to\infty) = \Delta p_0$. Furthermore, the elastic limit $t_R^{-1} \to 0$ yields

$$\widehat{\delta p}(s)_{\lim t_R^{-1}\to 0} = \frac{\Delta p_0 + s\tau\delta p_0^+}{s\tau(s+\tau^{-1})} \tag{A11}$$

which transforms to the elastic solution

$$\delta p_e(t) = \Delta p_0 + \left(\delta p_0^+ - \Delta p_0\right)e^{-t/\tau}, \tag{A12}$$

immediately seen to be the solution to (6).

The term in square brackets in the denominator of (A10) is quadratic in s, such that we rewrite (A10) as

$$\widehat{\delta p}(s) = \frac{\left(\Delta p_0 + s\tau\delta p_0^+\right)\left(s+t_R^{-1}\right)}{s\tau(s-s_1)(s-s_2)}, \tag{A13}$$

where the roots s_1, s_2 are

$$s_{1,2} = -\frac{t_R^{-1}(1+\mathcal{B}\alpha)+\tau^{-1}}{2} \pm \frac{1}{2}\sqrt{\left(t_R^{-1}(1+\mathcal{B}\alpha)+\tau^{-1}\right)^2 - 4\tau^{-1}t_R^{-1}}. \tag{A14}$$

Inverting the Laplace transform (A13) gives the chamber pressure in the time domain as in (9).

Note when $\mathcal{B} = 0$ (A10) reduces to the elastic solution (A11); in the perfectly compressible limit viscoelastic relaxation does not alter the chamber pressure. The roots $s_{1,2}$ correspond to $-\tau^{-1}$ and $-t_R^{-1}$.

In the no recharge limit $\tau^{-1} \to 0$, equation (A10) reduces to

$$\widehat{\delta p}(s)_{\lim \tau^{-1}\to 0} = \frac{\delta p_0^+}{s}\left(\frac{s+t_R^{-1}}{s+(1+\mathcal{B}\alpha)t_R^{-1}}\right), \tag{A15}$$

which transforms to equation (17).

A1. Surface Displacements

The displacements in the outer, elastic region are of particular interest since the free surface where measurements are made resides in region 2. From (A2) and (A3)

$$\hat{u}_r^{(2)}(r,s) = \frac{\widehat{\delta p}R_1^3}{4\mu r^2}\left(\frac{s+t_R^{-1}(R_2/R_1)^3}{s+t_R^{-1}}\right). \tag{A16}$$

These are the displacements in the outer, elastic full space. However, this result can be used to derive an approximate expression for displacements on the surface of a half-space in the limit that $R_2/d \ll 1$

[*Segall*, 2010, Chapter 7]. We follow the approach of *McTigue* [1987] for deriving the well-known Mogi solution for a spherical chamber in a fully elastic half-space. Resolving the displacements onto the plane $z = 0$ leads to vertical and horizontal (radial) displacements $u_z = u_r d/r$ and $u_h = u_r h/r$, where d is the depth of the chamber center, and h is the horizontal distance along the free surface measured from the projection of the chamber center. One can also resolve the radial stress in the full space into shear and normal tractions acting on the plane $z = 0$. *McTigue* [1987] applied equal and opposite tractions on $z = 0$ to render the plane traction free. Remarkably, this ends up simply increasing the displacements on $z = 0$ due to the full-space solution by a factor of $4(1-\nu)$. The solution is approximate in that the boundary conditions on the chamber wall and in the viscoelastic case the stresses within the shell are met only approximately. The traction boundary conditions on $z = 0$ are met exactly.

McTigue [1987] shows that at this stage the elastic solution is everywhere accurate to order $(R_1/d)^2$. He then derives a higher-order solution accurate to order $(R_1/d)^5$. While the elastic solution is only formally accurate for $R_1/d \ll 1$ the surface displacements are only modified by less than 10% for $R_1/d < 0.5$ when the next higher-order corrections are included. We may thus conjecture that the viscoelastic solution is reasonably accurate for $R_2/d \lesssim 0.5$, although further calculations are needed to confirm this. *McTigue* [1987, Figure 2b] shows that the deviatoric stresses are dominated by the spherically symmetric, full-space solution, even for $R_1/d = 0.5$, which suggests that viscoelastic displacements may also by reasonably well approximated by relaxation of these stresses.

Combining (A16) with (A13) and following the procedure described above yields

$$\hat{u}_z(z=0,s) = \frac{(1-\nu)R_1^3}{\mu d^2}\left[\frac{1}{(1+\zeta^2)^{3/2}}\right]\left\{\frac{\left(\Delta p_0 + s\tau\delta p_0^+\right)\left[s + t_R^{-1}(R_2/R_1)^3\right]}{s\tau(s-s_1)(s-s_2)}\right\}, \tag{A17}$$

where $\zeta = h/d$ is the radial distance from the center of the source normalized by the source depth. Horizontal displacements are found by multiplying by ζ. Equation (A17) can be inverted exactly; results are given in the main text, equation (15).

The limiting behavior is found by combining (A10) with (A16) and using the limit theorems for Laplace transforms, yielding $u(z=0, t=0^+) \propto \delta p_0^+ R_1^3/\mu d^2$ and $u(z=0, t\to\infty) \propto \Delta p_0 R_2^3/\mu d^2$. The infinite time response is also a Mogi solution, but with effective radius R_2 as the magma chamber pressure is transmitted to the boundary of the viscoelastic region in the fully relaxed state.

In the no recharge limit, $\tau^{-1} \to 0$, the surface displacements are found by combining (A16) and (A15)

$$\hat{u}_z(z=0,s)_{\lim \tau^{-1}\to 0} = \frac{(1-\nu)R_1^3}{\mu d^2}\left[\frac{1}{(1+\zeta^2)^{3/2}}\right]\frac{\delta p_0^+}{s}\left(\frac{s + t_R^{-1}(R_2/R_1)^3}{s + (1+\mathcal{B}\alpha)t_R^{-1}}\right), \tag{A18}$$

which has the inverse transform given by (18).

The case of $\mathcal{B} = 0$, $t_R = \tau$ is degenerate, $s_1 = s_2$. In this limit combining (A10) with (A16) leads to

$$\hat{u}_r^{(2)}(r,s) = \frac{R_1^3}{4\mu r^2}\frac{\left(\Delta p_0 + s\tau\delta p_0^+\right)\left(s + \tau^{-1}(R_2/R_1)^3\right)}{s\tau(s+\tau^{-1})^2}, \tag{A19}$$

which has inverse Laplace transform

$$\frac{4\mu r^2}{R_1^3}u_r^{(2)}(r,t) = \Delta p_0\left(\frac{R_2}{R_1}\right)^3 + e^{-t/\tau}\left\{\left(\delta p_0^+ - \Delta p_0\right)\left(\frac{t}{\tau}\left[\left(\frac{R_2}{R_1}\right)^3 - 1\right] + 1\right) - \Delta p_0\left[\left(\frac{R_2}{R_1}\right)^3 - 1\right]\right\}. \tag{A20}$$

A1.1. Convolution Form

It is worth noting from (A16) that the displacements in the exterior, elastic region can be written in the form of a convolution of the pressure rate with a viscoelastic kernel. The Laplace transform of $\mathrm{d}p/\mathrm{d}t$ is $s\widehat{\delta p} - \delta p_0^+$. Thus, the displacements can be written as

$$\hat{u}_r^{(2)}(r,s) = \frac{R_1^3}{4\mu r^2}\left[\mathcal{L}(\mathrm{d}p/\mathrm{d}t) + \delta p_0^+\right]\left[\frac{s + t_R^{-1}(R_2/R_1)^3}{s\left(s + t_R^{-1}\right)}\right], \tag{A21}$$

which in the time domain becomes

$$u_r^{(2)}(r,t) = \frac{\delta p_0^+ R_1^3}{4\mu r^2}\left[e^{-t/t_R} + \left(\frac{R_2}{R_1}\right)^3 (1 - e^{-t/t_R})\right] + \frac{R_1^3}{4\mu r^2}\int_0^t \frac{\mathrm{d}p(t')}{\mathrm{d}t'} \times \left\{\left(\frac{R_2}{R_1}\right)^3 + \left[1 - \left(\frac{R_2}{R_1}\right)^3\right] e^{-(t-t')/t_R}\right\} \mathrm{d}t'. \tag{A22}$$

A2. Stresses

The radial stresses for the *full-space solution* are given in the Laplace domain in *Segall* [2010] equation (7.102),

$$\hat{\sigma}_{rr}^{(1)} = -\frac{\widehat{\delta p}(s)}{s + t_R^{-1}}\left[\frac{sR_1^3}{r^3} + t_R^{-1}\right]$$
$$\hat{\sigma}_{rr}^{(2)} = -\frac{\widehat{\delta p}(s)R_1^3}{r^3}\left[\frac{s + t_R^{-1}(R_2/R_1)^3}{s + t_R^{-1}}\right]. \tag{A23}$$

The circumferential stresses are found from the strains, $\epsilon_{\theta\theta} = u_r/r$, and Hooke's law. Note that from the displacements (A2), the volumetric strain is $\hat{A}$ in region 1 and vanishes in region 2. Substituting the displacements into Hooke's law yields $\hat{\sigma}_{\theta\theta}^{(1)} = K_1\hat{A}(s) + 2\hat{\mu}(s)\hat{B}(s)/r^3$ and $\hat{\sigma}_{\theta\theta}^{(2)} = 2\mu\hat{C}(s)/r^3$, where K_1 is the bulk modulus of the inner region. Making use of the expressions (A3)

$$\hat{\sigma}_{\theta\theta}^{(1)} = \frac{\widehat{\delta p}(s)}{s + t_R^{-1}}\left[\frac{sR_1^3}{2r^3} - t_R^{-1}\right]$$
$$\hat{\sigma}_{\theta\theta}^{(2)} = \frac{\widehat{\delta p}(s)R_1^3}{2r^3}\left[\frac{s + t_R^{-1}(R_2/R_1)^3}{s + t_R^{-1}}\right]. \tag{A24}$$

To determine the general form of the stress, substitute (A13) into (A23) and (A24) and invert the transforms. The hoop stresses only are reported here as the radial stress follows similarly,

$$\sigma_{\theta\theta}^{(1)}(r,t) = -\frac{\Delta p_0}{\tau s_1 s_2 t_R} + \frac{(\Delta p_0 + s_1\tau\delta p_0^+)}{s_1\tau(s_1 - s_2)}\left(\frac{s_1 R_1^3}{2r^3} - t_R^{-1}\right)e^{s_1 t} + \frac{(\Delta p_0 + s_2\tau\delta p_0^+)}{s_2\tau(s_2 - s_1)}\left(\frac{s_2 R_1^3}{2r^3} - t_R^{-1}\right)e^{s_2 t}$$
$$\sigma_{\theta\theta}^{(2)}(r,t) = \frac{\Delta p_0}{2\tau s_1 s_2 t_R}\left(\frac{R_2}{R_1}\right)^3 + \frac{R_1^3}{2r^3}\left\{\frac{(\Delta p_0 + s_1\tau\delta p_0^+)}{s_1\tau(s_1 - s_2)}\left[s_1 + t_R^{-1}\left(\frac{R_2}{R_1}\right)^3\right]e^{s_1 t} + \frac{(\Delta p_0 + s_2\tau\delta p_0^+)}{s_2\tau(s_2 - s_1)}\left[s_2 + t_R^{-1}\left(\frac{R_2}{R_1}\right)^3\right]e^{s_2 t}\right\}. \tag{A25}$$

In the no recharge limit insert (A15) into (A23) and (A24) to get the stress

$$\hat{\sigma}_{\theta\theta\ \lim\tau^{-1}\to 0}^{(1)} = \frac{\delta p_0^+}{s\left[s + (1 + \mathcal{B}\alpha)t_R^{-1}\right]}\left[\frac{sR_1^3}{2r^3} - t_R^{-1}\right]$$
$$\hat{\sigma}_{rr\ \lim\tau^{-1}\to 0}^{(1)} = \frac{-\delta p_0^+}{s\left[s + (1 + \mathcal{B}\alpha)t_R^{-1}\right]}\left[\frac{sR_1^3}{r^3} + t_R^{-1}\right]. \tag{A26}$$

These invert to equation (29) in the main text.

Acknowledgments
This work grew out of a long ago discussion with Larry Mastin. Thanks also to Kyle Anderson and Andy Hooper for insightful discussions. The manuscript benefited substantially from suggestions of Associate Editor Mike Poland, reviewers Leif Karlstrom and Claude Jaupart. No data was used in this study. This work is supported by NSFEAR-1358607.

References

Dahlen, F., and J. Tromp (1998), *Theoretical Global Seismology*, Princeton Univ. Press, Princeton, N. J.
Del Negro, C., G. Currenti, and D. Scandura (2009), Temperature-dependent viscoelastic modeling of ground deformation: Application to Etna volcano during the 1993–1997 inflation period, *Phys. Earth Planet. Inter.*, *172*(3), 299–309.
Dragoni, M., and C. Magnanensi (1989), Displacement and stress produced by a pressurized, spherical magma chamber, surrounded by a viscoelastic shell, *Phys. Earth Planet. Inter.*, *56*(3), 316–328.
Dzurisin, D. (2003), A comprehensive approach to monitoring volcano deformation as a window on the eruption cycle, *Rev. Geophys.*, *41*(1).

Fialko, Y., Y. Khazan, and M. Simons (2001), Deformation due to a pressurized horizontal circular crack in an elastic half-space, with applications to volcano geodesy, *Geophys. J. Int.*, *146*(1), 181–90.

Hreinsdóttir, S., et al. (2014), Volcanic plume height correlated with magma-pressure change at Grimsvotn volcano, Iceland, *Nat. Geosci.*, *7*(3), 214–218.

Jellinek, A. M., and D. J. DePaolo (2003), A model for the origin of large silicic magma chambers: Precursors of caldera-forming eruptions, *Bull. Volcanol.*, *65*(5), 363–381.

Karlstrom, L., J. Dufek, and M. Manga (2009), Organization of volcanic plumbing through magmatic lensing by magma chambers and volcanic loads, *J. Geophys. Res.*, B10204, doi:10.1029/2009JB006339.

Karlstrom, L., J. Dufek, and M. Manga (2010), Magma chamber stability in arc and continental crust, *J. Volcanol. Geotherm. Res.*, *190*(3), 249–270.

Masterlark, T., M. Haney, H. Dickinson, T. Fournier, and C. Searcy (2010), Rheologic and structural controls on the deformation of Okmok volcano, Alaska: FEMs, InSAR, and ambient noise tomography, *J. Geophys. Res.*, B02409, doi:10.1029/2009JB006324.

Mastin, L. G., E. Roeloffs, N. M. Beeler, and J. E Quick (2008), Constraints on the size, overpressure, and volatile content of the Mount St. Helens magma system from geodetic and dome-growth measurements during the 2004–2006+ eruption, in *A Volcano Rekindled: The Renewed Eruption of Mount St. Helens, 2004–2006, chap. 22*, edited by D. R. Sherrod et al., pp. 461–488, U.S. Geol. Surv. Prof. Pap. 1750, Reston, Va.

McTigue, D. F. (1987), Elastic stress and deformation near a finite spherical magma body-resolution of the point-source paradox, *J. Geophys. Res.*, *92*(B12), 12,931–12,940.

Mogi, K. (1958), Relations between the eruptions of various volcanoes and the deformations of the ground surfaces around them, *Bull. Earthquake Res. Inst. Univ. Tokyo*, *36*, 111–123.

Newman, A., T. Dixon, G. Ofoegbu, and J. Dixon (2001), Geodetic and seismic constraints on recent activity at Long Valley Caldera, California: Evidence for viscoelastic rheology, *J. Volcanol. Geotherm. Res.*, *105*(3), 183–206.

Newman, A. V., T. H. Dixon, and N. Gourmelen (2006), A four-dimensional viscoelastic deformation model for Long Valley Caldera, California, between 1995 and 2000, *J. Volcanol. Geotherm. Res.*, *150*(1), 244–269.

Nooner, S. L., and W. W. Chadwick (2009), Volcanic inflation measured in the caldera of Axial seamount: Implications for magma supply and future eruptions, *Geochem. Geophys. Geosyst.*, *10*, Q02002.

Reverso, T., J. Vandemeulebrouck, F. Jouanne, V. Pinel, T. Villemin, E. Sturkell, and P. Bascou (2014), A two-magma chamber model as a source of deformation at Grimsvötn volcano, Iceland, *J. Geophys. Res. Solid Earth*, *119*, 4666–4683, doi:10.1002/2013JB010569.

Rubin, A. M. (1993), On the thermal viability of dikes leaving magma chambers, *Geophys. Res. Lett.*, *20*(4), 257–260.

Segall, P. (2010), *Earthquake and Volcano Deformation*, Princeton Univ. Press, Princeton, N. J.

Segall, P. (2013), Volcano deformation and eruption forecasting, in *Remote Sensing of Volcanoes and Volcanic Processes: Integrating Observation and Modelling*, edited by D. M. Pyle, T. A. Mather, and J. Biggs, vol. 380, pp. 85–106, Geol. Soc. Spec. Publ., London.

Sturkell, E., P. Einarsson, F. Sigmundsson, H. Geirsson, H. Olafsson, R. Pedersen, E. de Zeeuw-van Dalfsen, A. Linde, S. Sacks, and R. Stefánsson (2006), Volcano geodesy and magma dynamics in Iceland, *J. Volcanol. Geotherm. Res.*, *150*(1–3), 14–34.

Sturkell, E., K. Ágústsson, A. T. Linde, S. I. Sacks, P. Einarsson, F. Sigmundsson, H. Geirsson, R. Pedersen, P. C. LaFemina, and H. Ólafsson (2013), New insights into volcanic activity from strain and other deformation data for the Hekla 2000 eruption, *J. Volcanol. Geotherm. Res.*, *256*, 78–86.

Yang, X. M., P. M. Davis, and J. H. Dieterich (1988), Deformation from inflation of a dipping finite prolate spheroid in an elastic half-space as a model for volcanic stressing, *J. Geophys. Res.*, *93*(B5), 4249–4257, doi:10.1029/JB093iB05p04249.